



CHORUS

This is the accepted manuscript made available via CHORUS. The article has been published as:

Strongly Emitting Surfaces Unable to Float below Plasma Potential

M. D. Campanell and M. V. Umansky

Phys. Rev. Lett. **116**, 085003 — Published 25 February 2016

DOI: [10.1103/PhysRevLett.116.085003](https://doi.org/10.1103/PhysRevLett.116.085003)

Strongly Emitting Surfaces Unable to Float Below Plasma Potential

M.D. Campanell and M.V. Umansky

Lawrence Livermore National Laboratory, P.O. Box 808(L-630), Livermore, CA 94551, USA

An important unresolved question in plasma physics concerns the effect of strong electron emission on plasma-surface interactions. Previous papers reported solutions with negative and positive floating potentials relative to the plasma edge. The two models give very different predictions for particle and energy balance. Here we show that the positive potential state is the only possible equilibrium in general. Even if a negative floating potential existed at $t=0$, the ionization collisions near the surface will force a transition to the positive floating potential state. This transition is demonstrated with a new simulation code.

Understanding plasma-surface interaction with strong electron emission is an important fundamental problem relevant to laboratory and astrophysical plasmas [1]. Two distinct equilibrium states in planar geometry have been proposed in the literature. In conventional “space-charge limited” (SCL) sheath models, the wall potential is negative relative to the plasma edge [2,3,4]. A presheath potential accelerates ions to the Bohm speed at the edge. These model assumptions are widely used when estimating floating potentials, sputtering rate and energy flux at strongly emitting divertor plates [5], plasma thruster walls [6], probe diagnostics [7,8] and large dust particles [9].

Recent theory [10] and simulation [11,12,13] studies have demonstrated a second solution type. In the “inverse regime” the sheath potential is positive, opposite in sign from the SCL. An inverted presheath has a force balance unrelated to Bohm presheaths [14]. The particle and energy fluxes in the inverse regime are much different from the SCL regime.

Because the two models are so different, it is essential to determine when each one applies. Thermionic emission from hot metals [15] and photoemission from sunlight exposure [16] can induce a “strong” emitted flux Γ_{emit} that exceeds the influx of electrons from the plasma Γ_{ep} . Secondary emission coefficients $\gamma \equiv \Gamma_{emit}/\Gamma_{ep}$ can exceed unity for metal surfaces [17] at high plasma temperatures while dielectric surfaces or oxide film coated electrodes [18] have significantly higher emission yields which can enable $\gamma > 1$ at more modest temperatures. For any emission type when $\gamma > 1$, the zero current condition cannot be met unless some of the emission is returned to the wall by a barrier field ($\Gamma_{eret} > 0$).

$$\Gamma_{ep}(1 - \gamma) + \Gamma_{eret} = \Gamma_i \geq 0 \quad (1)$$

The theoretical potential distributions $\phi(x)$ near the wall for each γ are sketched in Fig. 1 (see Ref. [10] for further discussion). For $\gamma > 1$, the SCL and inverse models both give valid solutions with the required emission barrier. Does this mean both states could exist in applications?

In this Letter we show that only the inverse equilibrium is possible when $\gamma > 1$. The reason stems from the fact that the SCL solution has a potential “dip”. In general, potential wells in plasmas collect cold ions born by e-n ionization or i-n charge exchange collisions. The accumulated ion space

charge then smooths out the wells. This was demonstrated in experiments with tandem mirrors [19], heated cathodes [20] and positively biased anodes [21].

If a SCL-like $\phi(x)$ did exist at $t=0$, one may expect the equilibrium $\phi(x)$ after ion accumulation to look like the red dashed curve in Fig. 1, with ϕ_{wall} similar to before. However, floating condition (1) could not be sustained if $\gamma > 1$ because there is no emission barrier ($\Gamma_{eret} = 0$). The wall would lose electrons, making ϕ_{wall} increase to recreate a dip (green dotted curve). As ions keep accumulating in the dip, ϕ_{wall} will be forced more and more positive. This will drive a transition to the inverse regime.

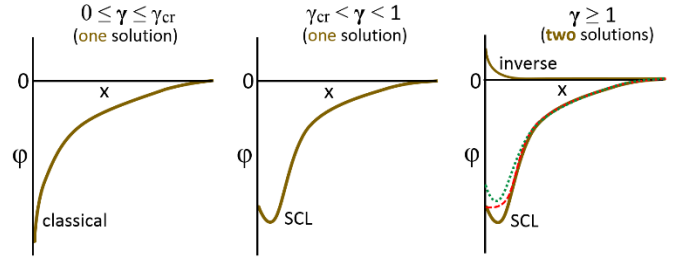


FIG. 1: Qualitative sketch of the $\phi(x)$ solution for each γ range, based on *collisionless* theories. The change from classical to SCL occurs at a critical γ_{cr} near unity. Then when γ exceeds unity, there are two solutions, a SCL and an inverse. A small rate of ionization will not disrupt classical or inverse sheaths because they expel ions. But cold ions will accumulate in the SCL “dip”.

Although the SCL theory has been supported over the years by numerical simulations, the SCL was only seen in source boundary injection simulations without collisions [2,3,4,22,23]. If collision effects such as ionization are included in the volume, the outcome will be much different. We wrote a new program that solves the kinetic equations on a uniform 1D-1V grid between two planar boundaries. Ions and electrons start with a spatially uniform Maxwellian velocity distribution function (VDF) f_0 , with different masses and temperatures, and equal density N_0 .

$$f_0(x, v) = N_0 \sqrt{\frac{m}{2\pi T}} \exp\left(\frac{-mv^2}{2T}\right) \quad (2)$$

At each time step, f_i and f_e are advanced explicitly in four stages according to the kinetic equation (3). Upwind finite difference derivatives are taken for the advections. The electric field $E(x)$ is evaluated by setting $E = 0$ at the midplane by symmetry and integrating $(n_i - n_e)$.

$$\frac{\partial f}{\partial t} = -v \frac{\partial f}{\partial x} - \frac{qE}{m} \frac{\partial f}{\partial v} + S_{charge} + S_{coll} \quad (3)$$

Charge source S_{charge} produces equal quantities of ions and electrons uniformly in space with the same temperatures as their initial state (2). To fix the plasma density as an independent variable, the source intensity is feedback controlled to offset the wall flux losses, thereby maintaining a spatially averaged density equal to N_0 .

$$S_{charge} = \frac{2\Gamma_i}{N_0 L} f_0 \quad (4)$$

S_{coll} is a BGK type collision operator. Although it does not rigorously model interparticle collisions, it is convenient for simulating the general effects of collisions on plasma-wall interaction. A similar operator was successfully used to simulate magnetic sheath and presheath [24].

$$S_{coll} = C \left(\frac{n}{N_0} f_0 - f \right) \quad (5)$$

S_{coll} acts to relax the electron and ion VDF's at each x to a Maxwellian with the same temperature as the initial states. For electrons, S_{coll} serves as the heating mechanism that repopulates the energetic tail lost to the walls. It also thermalizes the emitted electrons. For ions, S_{coll} acts to drag accelerated ions like charge exchange friction (although a collision rate proportional to v would be more accurate for charge exchange [25]). Here, the collision rate C is set to a moderate value such that electrons moving at the thermal speed $v_{Te} \equiv (T_e/m_e)^{1/2}$ and ions moving at sound speed $c_s \equiv (T_e/m_i)^{1/2}$ suffer a few collisions per transit time.

For boundary conditions, the plasma-facing part of the IVDF at each wall is set to zero. The emitted electron VDF is Maxwellian, $\sim A \exp(-m_e v^2 / 2T_{emit})$. At each time step, A is updated so that the emitted flux Γ_{emit} equals the chosen γ times the plasma electron influx Γ_{ep} . The influx is recorded at the minimum of $\phi(x)$ so that if an emission barrier is present, the returned electrons Γ_{eret} do not induce emission (although repeated reflections of the low energy electrons could be possible for some materials in light of Ref. [26]).

Advancing the DF's from the uniform initial state (2), the system evolves to an equilibrium with well-defined sheath and quasineutral presheath regions. Output data is free from the numerical noise that often obscures PIC simulation results. Spatial grids are set to ensure good resolution of the sheaths. Separate velocity grids are used for electrons and ions, enabling good resolution of their characteristic speeds.

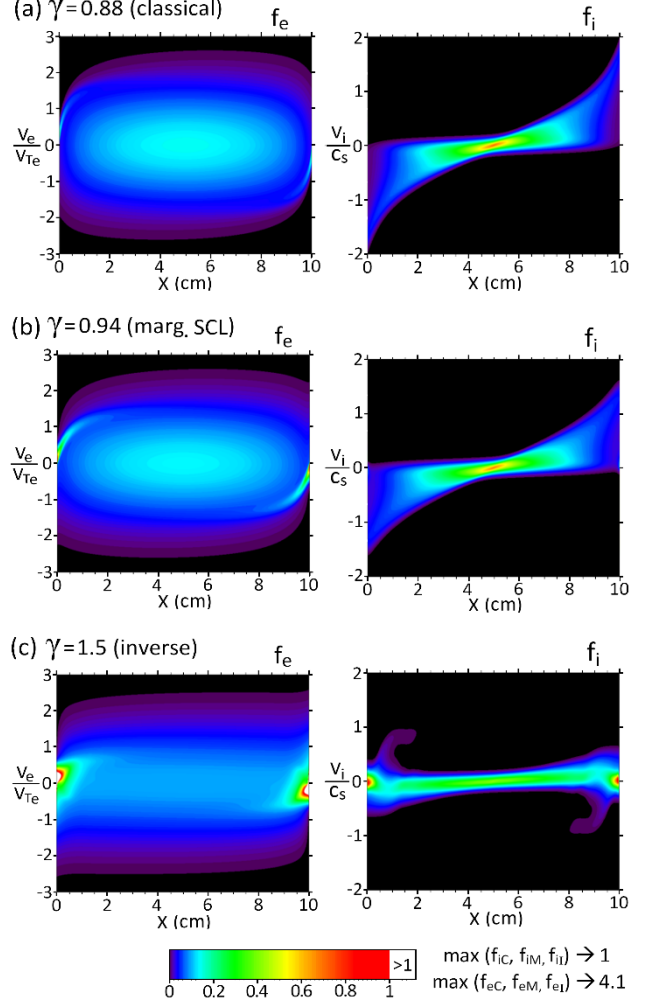


FIG. 2. Equilibrium solutions for three representative γ values. All IDF's use the same color scale shown. The largest f_i value among the three runs is mapped to 1. EDF's also use the same scale except the largest value among the three f_e 's is mapped to 4.1.

Figure 2 gives the equilibrium distribution functions representing the different emission regimes. Other output data are plotted in Fig. 3. Independent physical parameters are $N_0 = 3.5 \times 10^{14} \text{m}^{-3}$, $T_e = 20 \text{eV}$, $T_{emit} = 1 \text{eV}$, $m_i = 1 \text{amu}$, $L = 10 \text{cm}$, $T_i = 0.1 \text{eV}$, $C_e = 8v_{Te}/L$, $C_i = 3c_s/L$. Numerical parameters are $n_x = 1001$, $n_v = 300$, $t_{step} = 10^{-11} \text{s}$, $|v_{e,max}| = 4(T_e/m_e)^{1/2}$, $|v_{i,max}| = 2(T_e/m_i)^{1/2}$. Under these conditions, $\phi_{wall} = -75 \text{V}$ when $\gamma = 0$. As γ is raised, $|\phi_{wall}|$ decreases to allow more plasma electrons to reach the wall to maintain (1).

Fig. 2(a) gives the solution for $\gamma = 0.88$. The EDF's elliptical contours indicate that most bulk electrons are confined. The IDF shows how the ion speeds at each x range from ~ 0 to some maximum value which increases towards the walls due to the accelerating potential fall. The potential $\phi_C(x)$ in Fig. 3(b) is classical monotonic with $\phi_{wall} = -33.5 \text{V}$. The net charge in the classical sheath is positive, Fig. 3(a).

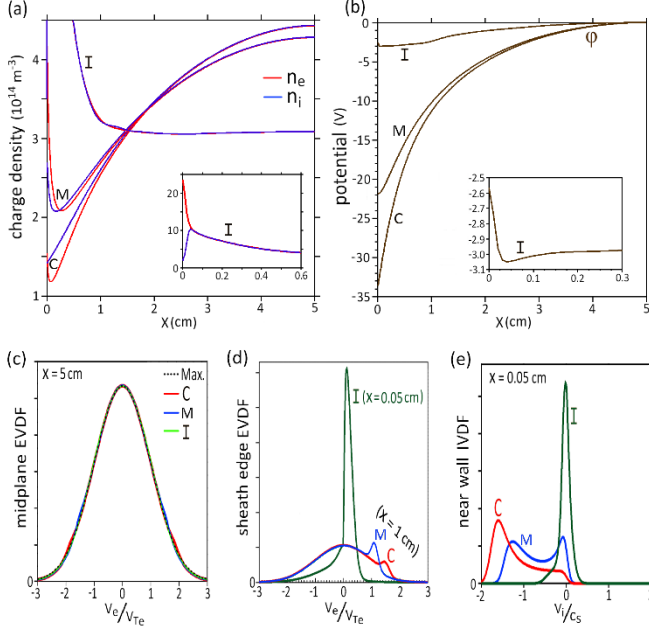


FIG. 3. Profiles of (a) charge density and (b) potential in the classical “C”, marginal “M” and inverse “I” runs. (c) Midplane EVDF’s compared to a 20eV Maxwellian. (d) EVDF’s at the presheath-sheath edge. The inverse edge is at $x = 0.05 \text{ cm}$. We use $x_{\text{edge}} = 1 \text{ cm}$ for the C and M sheaths although the edge is not sharp in these states. (e) IVDF’s at $x = 0.05 \text{ cm}$. Because the VDF’s in (c-e) are normalized to the density at the given point, making the area under each curve equal.

As γ nears unity, an intense negative charge layer from emitted electrons develops in the sheath, causing the electric field at the wall to weaken. At $\gamma_{\text{cr}} = 0.94$, $d\phi/dx \approx 0$ at the wall, Fig. 3(b). Compared to Fig. 2(a), the DF’s in the “marginal SCL” state in Fig. 2(b) look similar except the emitted beam intensity is far larger and the maximal ion speed smaller (due to the smaller $|\phi_{\text{wall}}| = 22 \text{ V}$). In the EDF, one can see how the emitted beams get accelerated away and thermalize. Note how most of the difference between $\phi_C(x)$ and $\phi_M(x)$ in Fig. 3(b) is in the sheath region, $x \in [0, 1 \text{ cm}]$. The presheath drop between $x = 1 \text{ cm}$ and 5 cm changes only from -11.5 to -10 V , supporting the conventional idea that the presheath is insensitive to γ [27].

When $\gamma > \gamma_{\text{cr}}$, conventional theories predict a potential dip will form but the net sheath and presheath potentials will be similar to when $\gamma = \gamma_{\text{cr}}$. Instead when we simulate $\gamma = 1.5$, the DF’s in Fig. 2(c) are nothing like the marginal SCL; there is no bulk electron confinement, no ion acceleration and no acceleration of the emission. The sheath potential is now positive 0.5 V , see Fig. 3(b) insert. The plasma density now *increases* from the midplane to the edge because when the sheath potential is positive, the right half of the EVDF at the edge ($x=0.05 \text{ cm}$) contains *only* cold electrons from the wall, which build up a high density due to their low speed, see Fig. 3(d). By comparison in the C and M states, the edge EVDF is dominated by hot electrons and the emitted beam produces

only a small peak after their acceleration in the negative sheath potential. Note that the emitted beams are well thermalized by the BGK collisions before reaching the midplane. The midplane EVDF is close to a 20eV Maxwellian in each run, Fig. 3(c).

When benchmarking the new code, we verified that the equilibrium states vary as theoretically expected with parameters like density, temperatures and collisionality. For any plasma properties, the sheaths and presheaths are always inverse when $\gamma > 1$. The main result we want to demonstrate here is *why* SCL-like states never appear. We will attempt to force the plasma into a SCL state by starting a new run with the DF’s in the marginal SCL equilibrium of Fig. 2(b) and then increasing γ to 1.5 at $t = 0$.

The ensuing temporal evolution is shown in Fig. 4. A potential dip of amplitude $\sim 0.6 \text{ V}$ forms within 4ns, Fig. 4(a). The wall potential ϕ_{wall} oscillates and appears to stabilize within 50ns. So far at $t = 50 \text{ ns}$, the outcome is consistent with SCL theories. The $\phi_{\text{wall}} = -20.6 \text{ V}$ is close to the marginal SCL value (-21.8 V). The dip formation has perturbed the electric field and charge densities only right near the wall, Fig. 4(b,e). The dip just blocks the extra emission so that $\gamma_{\text{eff}} \approx \gamma_{\text{cr}} < 1$, maintaining current balance. In the interior plasma, electrons and ions are created and lost to the boundaries at nearly the same rates as before. However, ions created in the $\sim 0.1 \text{ cm}$ -wide dip region are now getting trapped there.

Over a longer time scale, a second transition occurs. In Fig. 4(c), a peak emerges in $n_i(x)$ around the dip region. The IVDF in the dip in Fig. 4(d) shows the ion density growth is from cold unaccelerated ions. As the ions accumulate, ϕ_{wall} gets driven upwards, Fig. 4(e). The sheath which started as a double layer at $t = 0$ is by $t = 2 \mu\text{s}$ a 0.05 cm -wide single layer of net negative charge, Fig. 4(c). Overall, the SCL sheath has transitioned to an inverse sheath while simultaneously the Bohm presheath transitioned to an inverted presheath, causing the entire plasma mass to shift towards the walls. We confirmed that this transition does not occur if S_{coll} and S_{charge} are turned off within 0.15 cm of the walls. A steady SCL can be sustained in our simulations with $\gamma > 1$ only if no cold ions are created in the dip.

When the transition is complete, the final DF’s are identical to Fig. 2(c). It is important to mention that a static equilibrium is not reached in this inverse regime because of two-stream instabilities [28] excited by the intense emitted beams. (Other sheath related instabilities can prevent static plasma-wall interactions [29].) For clarity, we plotted time-averaged data for the inverse run in Figs. 2 and 3. Despite the major charge imbalances in the region around $x = 0.7 \text{ cm}$ in individual snapshots (see Fig. 4c at $t = 2 \mu\text{s}$), this region is quasineutral on average.

The waves are still significant because they impart extra thermal energy to the ions, affecting the force balance. In the inverse run the (-3 V) presheath drop does not significantly accelerate the ions, Fig. 3(e). The fundamental purpose of the presheath electric field is to offset the pressure gradient created by the ion density gradient and thermal energy.

Because the $-3V$ presheath drop exceeds the inverse sheath ($+0.5V$), the wall actually floats negative relative to parts of the upstream plasma even though it floats positive relative to the plasma *edge*. Hence it is important to note for experimental consideration that a negative ϕ_{wall} or nonmonotonic $\phi(x)$ cannot by itself determine whether a state is SCL or inverse. Other measurements such as charge density gradients could distinguish the states, c.f. Fig. 3(a).

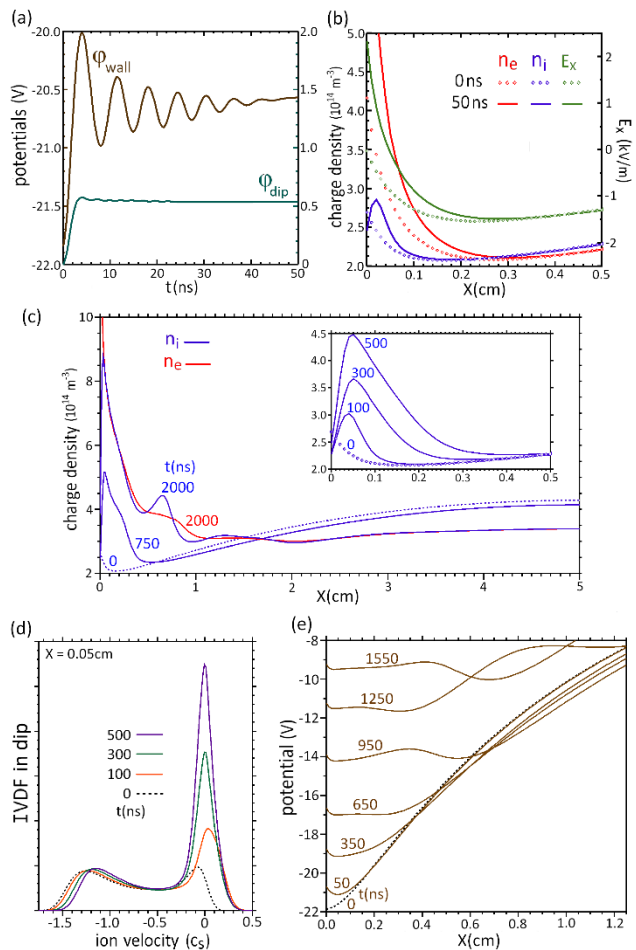


FIG. 4. Time evolution after γ is raised from 0.94 to 1.5. (a) Initial evolution of ϕ_{wall} and ϕ_{dip} during dip formation. (b) Charge and E field profiles before and after dip formation. (c) Long term evolution of $n_i(x)$. (d) Long term evolution of the IVDF at a point in the dip. (e) Potential snapshots during the transition. Note that most ordinates in this figure start at nonzero values.

The fact that $\phi_i(x)$ is nonmonotonic in Fig. 3(c) may appear at odds with our premise that a SCL equilibrium is impossible due to the dip in $\phi_{\text{SCL}}(x)$. The key difference in the inverse regime is the *sheath* is monotonic and the “dip” extends into the quasineutral plasma. Cold ions created in the inverse sheath just accelerate into the plasma and thermalize. A SCL regime gets destroyed because ions build up inside the sheath and begin to neutralize the emission barrier.

It is reasonable to conclude that the inverse regime should prevail over the SCL in general. In experiments, sheaths always contain cold neutrals from background gas or wall recycling. Both e-n ionization and i-n charge exchange can produce the cold ions which destroy SCL states. We now see why stable SCL’s were only seen in simulation models without ionization [2,3,4]. A SCL might be sustainable experimentally if ions created near a $\gamma > 1$ surface are “pumped” by escaping in the dimension parallel to the surface. This could be ruled out in magnetized systems like divertors because the \mathbf{B} field would inhibit such an escape.

Ion escape can also be ruled out if $\gamma > 1$ on the whole surface. A possible implication is that emissive probes float at positive potentials rather than the negative (SCL) potential often assumed when using the floating point measurement method [7]. A positive floating potential of an emissive probe was actually reported in Ref. [30]. However we note that our study only directly applies to thin (planar geometry) sheaths. Future studies can explore possible connections to curved emitting objects like dust grains in the fundamentally different orbital motion limited [31] and weakly screened [32] cases. Interestingly, potential wells have been observed around strongly emitting, positively charged dust grains in OML regime simulations without collisions [33]. So we can suggest that ion accumulation in the wells might significantly alter the screening potential and surface charge.

Further measurements are needed to identify the emission regimes in applications. Some interesting fundamental experiments on emission were conducted [3,20,34,35], but it is difficult to conclude whether the SCL or inverse regime was present from the available data. For example in Ref. 34, the authors compared measurements to a SCL model and reported major discrepancies. The lack of ion acceleration and increase of plasma density towards the strongly emitting plate (see their Fig. 6 and Table I) are more consistent with inverse theory.

This work was performed under the auspices of the U.S. Department of Energy by Lawrence Livermore National Laboratory under Contract No. DE-AC52-07NA27344. This material is based upon work supported by the U.S. Department of Energy.

[1] S. Robertson, Plasma Phys. Contr. Fusion **55**, 093001 (2013).
[2] L. A. Schwager, Phys. Fluids B: Plasma Physics **5**, 631 (1993)
[3] J. P. Sheehan, N. Hershkowitz, I. D. Kaganovich, H. Wang, Y. Raites, E. V. Barnat, B. R. Weatherford, and D. Sydorenko, Phys. Rev. Lett. **111**, 075002 (2013).
[4] N. Rizopoulou, A. P. L. Robinson, M. Coppins, and M. Bacharis, Phys. Plasmas **21**, 103507 (2014).
[5] P. C. Stangeby, The Plasma Boundary of Magnetic Fusion Devices, Plasma Physics Series (IOP, Bristol, 2000).
[6] K. Hara, M. J. Seakerak, I. D. Boyd, and A. D. Gallimore, J. Appl. Phys. **115**, 203304 (2014).
[7] M.J. Martin, J. Bonde, W. Gekelman and P. Pribyl, Review of Scientific Instruments **86**, 053507 (2015).
[8] A. Fruchtman, D. Zoler, and G. Makrinich, Phys. Rev. E **84**, 025402(R) (2011).

-
- [9] M. Bacharis, *Phys. Plasmas* **21**, 074501 (2014).
- [10] M. D. Campanell, *Phys. Rev. E* **88**, 033103 (2013).
- [11] M. D. Campanell, A. V. Khrabrov, and I. D. Kaganovich, *Phys. Rev. Lett* **108**, 255001 (2012).
- [12] F. Taccogna, *Eur. Phys. J. D* **68**, 199 (2014).
- [13] C-W Huang, Y-C Chen and Y. Nishimura, *IEEE Trans. Plasma Sci.* **43**, 675 (2015).
- [14] M.D. Campanell, *Phys. Plasmas* **22**, 040702 (2015).
- [15] L. A. Schwager, W. L. Hsu, and D. M. Tung *Phys. Fluids B: Plasma Physics* **5**, 621 (1993).
- [16] W.M. Farrell, A.R. Poppe, M.I. Zimmerman, J.S. Halekas, G.T. Delory, and R.M. Killen, *J. Geophys. Res.: Planets* **118**, 1114 (2013).
- [17] C.A. Ordonez and R.E. Peterkin, *J. Appl. Phys.* **79**, 2270 (1996).
- [18] K.M. Gutorov, I.V. Vizaglov, E.A. Markina and V.A. Kurnaev, *Bull. Russian Acad. Sciences: Physics* **74**, 188 (2010).
- [19] D.E. Baldwin and B.G. Logan, *Phys. Rev. Lett.* **43**, 1318 (1979).
- [20] T. Intrator, M. H. Cho, E. Y. Wang, N. Hershkowitz, D. Diebold, and J. DeKock, *J. Appl. Phys.* **64**, 2927 (1988).
- [21] C. Forest and N. Hershkowitz, *J. Appl. Phys.* **60**, 1295 (1986).
- [22] S. Ishiguro and N. Sato, *J. Phys. Sot. Jpn.* **60**, 2218 (1991).
- [23] T. Gyergyek and J. Kovačič, *Phys. Plasmas* **19**, 013506 (2012).
- [24] D. Coulette and G. Manfredi, *J. Phys.: Conf. Ser.* **561**, 012005 (2014).
- [25] M. Lampe, T.B. Röcker, G. Joyce, S.K. Zhdanov, A.V. Ivlev and G.E. Morfill, *Phys. Plasmas* **19**, 113703 (2012).
- [26] F. X. Bronold and H. Fehske, *Phys. Rev. Lett.* **115**, 225001 (2015).
- [27] G. D. Hobbs and J. A. Wesson, *Plasma Phys.* **9**, 85 (1967).
- [28] D. Sydorenko, A. Smolyakov, I. Kaganovich, and Y. Raitses, *Phys. Plasmas* **14**, 013508 (2007).
- [29] A. I. Smolyakov, W. Frias, I. D. Kaganovich and Y. Raitses, *Phys. Rev. Lett.* **111**, 115002 (2013).
- [30] C. Ionita, et al., *Contrib. Plasma Phys.* **51**, 264–270 (2011).
- [31] G. L. Delzanno and X. Tang, *Phys. Rev. Lett.* **113**, 035002 (2014).
- [32] D.I. Zhukhovitskii, O.F. Petrov, T.W. Hyde, G.Herdrich, R. Laufer, M. Dropmann, L.S. Matthews, *New J. Phys.* **17**, 053041 (2015).
- [33] G. L. Delzanno, G. Lapenta, and M. Rosenberg, *Phys. Rev. Lett.* **92**, 035002 (2004).
- [34] L. A. Schwager, W. L. Hsu, and M. D. Tung, *Phys. Fluids B* **5**, 621–630 (1993).
- [35] I.V. Schweigert, S.J. Langendorf, M. L. R. Walker and M Keidar *Plasma Sources Sci. Technol.* **24**, 025012 (2015).